

Received November 14, 2021, accepted November 29, 2021, date of publication December 3, 2021, date of current version December 20, 2021.

Digital Object Identifier 10.1109/ACCESS.2021.3132645

# Tightly Coupling Fusion of UWB Ranging and IMU Pedestrian Dead Reckoning for Indoor Localization

RASHID ALI<sup>1,2</sup>, RAN LIU<sup>1</sup>, ANAND NAYYAR<sup>3,4</sup>, BASIT QURESHI<sup>5</sup>, (Member, IEEE), AND ZHIQIANG CAO<sup>1</sup>

<sup>1</sup>School of Information Engineering, Southwest University of Science and Technology, Mianyang 621010, China

<sup>2</sup>Department of Computer Science, University of Turbat, Kech, Turbat, Balochistan 92600, Pakistan

<sup>3</sup>Graduate School, Duy Tan University, Da Nang 550000, Vietnam

<sup>4</sup>Faculty of Information Technology, Duy Tan University, Da Nang 550000, Vietnam

<sup>5</sup>Department of Computer Science, Prince Sultan University, Riyadh 11586, Saudi Arabia

Corresponding authors: Rashid Ali (alirashid@mails.swust.edu.cn) and Anand Nayyar (anandnayyar@duytan.edu.vn)

This work was supported in part by the Robotics and Internet of Things Laboratory, Prince Sultan University, Riyadh, Saudi Arabia.

**ABSTRACT** Ultra-wideband (UWB) and inertial measurement unit (IMU) fusion is an efficient method to resolve the uncertainties of UWB in non-line-of-sight (NLOS) situations because of signals refraction, the effect of multipath and inertial positioning error accumulation in indoor environments. Existing systems, however, are focused only on foot-mounted IMUs that restrict the system's implementation to particular real situations. In this research, using foot-mounted IMU, we suggest combining UWB ranging and IMU pedestrian dead reckoning (PDR), which can provide a generic indoor positioning solution. The issues such as position and orientation drift, interferences and divergence in strap-down inertial navigation system (SINS) based orientation estimates could be addressed by a UWB ranging sensor fusing with an IMU using the extended Kalman filter (EKF). The main goal of this research is to investigate and compare two different sensor data fusion techniques. For instance, adaptive Kalman filter (AKF) and least-squares (LSs) incorporate a foot-mounted IMU tightly coupled to a 2D pedestrian positioning solution derived from UWB signals. Moreover, we consider the UWB NLOS and IMU error identification. A real-time ranging error compensation model based on the LS method and AKF positioning algorithm are used for fixing such problems. We propose a new tightly coupled inertial navigation system (INS) with a two-way ranging (TWR) fusion positioning algorithm to improve accuracy, integrating UWB and IMU sensors based on the EKF in pedestrian navigation. Experiments in dynamic indoor environment validate the effectiveness of the proposed approach that uses EKF to combine AKF and LS for error minimization.

**INDEX TERMS** Foot-mounted IMU, pedestrian, indoor navigation, EKF, tightly coupling, UWB.

## I. INTRODUCTION

The global positioning system (GPS) is the most advanced outdoor positioning system in recent years. However, the signal strength is in the microwave frequency range, and when it hits the ground, the signal intensity becomes poor and does not penetrate in a certain indoor environment [1]. Thus, for indoor positioning scenarios, GPS is not feasible. In general, 80% of human activities are in an indoor environment, and the demand for indoor positioning is far higher than for outdoor placement. So, indoor pedestrian navigation (IPN)

The associate editor coordinating the review of this manuscript and approving it for publication was Dušan Grujić.

and positioning is considered to be one of the important tools for persons to find their routes in wide indoor environments such as libraries, parking lots, warehouses, shopping malls, patient tracking in hospitals, fire emergency in a building, etc. More importantly, the requirements can be met in PDR on the basis of UWB/IMU. The PDR is based on pedestrian patterns and uses IMU sensors that include an accelerometer and a gyroscope. PDR's core features for calculating relative motions are the estimation of stride length, heading estimation and step detection. Mainly, PDR uses IMU sensors to determine a user's momentary movements and estimates the user's present position by iteratively combining the simultaneous movements to the prior position. In [50],

PDR can predict location with reasonable accuracy over short time intervals, but it causes the IMU sensors to suffer from cumulative errors as time passes. Moreover, PDR accuracy is dependent on the precision of the prior position and the IMU sensors; different assisting techniques can help PDR to perform better.

For government security and commercial purposes, high-precision location data plays an important role. Positioning technology is also commonly used in vehicle navigation, search and rescue, health tracking, identification of logistics targets, and other areas. The massive demand for location services has spawned wireless communication and network technologies such as UWB, Bluetooth, wireless fidelity (WiFi), radio-frequency identification (RFID), and Zigbee [2], [43], [54]. Moreover, the INS enhances the combined navigation in challenging environments, and range observation has been expressed in GPS/INS tightly coupled navigation through UWB with an improved robust Kalman filter [3]. A system that uses low-cost UWB measurement techniques to enhance the UWB/micro-electromechanical systems (MEMS) IMU navigation has been suggested, for instance, in an environment where the UWB positioning system has been presented. Cardarelli *et al.* [55] proposed a single IMU sensor and estimated the 3D human body centre of mass (CoM) displacement by a method of the sacral marker during treadmill walking and achieved a reliable estimation during cyclic activities using the UKF; to focus on data accuracy with instrumentation of low-cost instead of real-time applicability to avoid orientation estimation errors. A multi-sensor fusion technique has been produced while a dynamic location accuracy of 20 cm was achieved during the UWB range measurements [44]. An EKF was applied to the GPS observations, and the UWB ranges tightly coupled method explained the additional error states and the systematic UWB errors in real-time [5]. There are two ways to realize wireless positioning, the received signal strength indicator (RSSI) and time of flight (TOF). The RSSI algorithm, also known as the fingerprint method, uses the wireless signal's energy attenuation model to propagate in the channel to estimate the distance.

In [52], the GPS/INS community recognizes that the loose paradigm is less efficient than some other systems incorporating raw sensory data at such low process levels as tight integration, which are drift reduction with the availability of one node, i.e., the existence of RSS measurement. The sensor error features such as IMU biases, model parameters, among many other factors, are some of the advantages of tightly coupling integrations. A tightly coupling method in [51] is proposed by implementing a Kalman filter (KF) with INS/RFID utilizing the predicted INS range to tag between the residual. The technique incorporates zero-velocity updates (ZUPTs) for foot stances, zero-angular rate updates (ZARUs) for still phases, and heading drift reduction (magnetometer). The loosely coupled model is a low-level paradigm in which the integration of sub positioning technologies operates independently. The loosely coupling paradigm has the merit of

overcoming the thresholds of sub positioning techniques for integration and is relatively easy to implement [45]. Even though it might be figured out that the loosely coupled model's accuracy will ultimately be limited over time, such a sub positioning system may not provide the position data. On the other hand, the tightly coupling model is suggested as a supporting system to overcome this drawback [22], [42]. In addition, the most extensively used data fusion filtering algorithms, such as EKF, are built on KF to provide state estimation via the data fusion paradigm [13]. There seems to be some literature on merging UWB and inertial navigation sensors to the researcher's knowledge. The recent works incorporate a hybrid 2D location tracking technique [46] and an EKF for pedestrian tracking [47]. A loosely coupling paradigm is defined as a system in which the data through one or more different sensors is pre-processed before calculating the final results, which have a minimal number of degrees of freedom (DOF) IMU to estimate and act separately. A tightly coupling paradigm is one in which all estimations are used to obtain the final results immediately.

In the cases of fewer anchors, the tightly coupled model can also be used by applying raw UWB/IMU information mechanization algorithms in an EKF. So UWB/IMU tightly coupled navigation is more flexible. Because the tightly coupled system was significantly more accurate, robust, jam-resistant, and less costly, a reconfigurable UWB/IMU tightly coupled navigation filter was designed for spacecraft application [6]. The range measurement data collected with widely deployed UWB radio frequencies under optimum line-of-sight (LOS) conditions are evaluated with assessed distances using conventional UWB error assessment methods [5]. For the simultaneous reconstruction of the Human body (attitude and displacement), Qiu *et al.* [56] presented a low-cost IMU motion capture and lightweight ZUPT technique, which distributes fifteen sensor nodes on the human limbs for calculating foot displacement. The INS can calculate the current attitude (or orientation), velocity and location of the system using the IMU measurements starting from some known initial point. However, as time increases, the computed navigation states such as velocity, position and attitude can rise due to their long-term drifts, like the gyroscopes or accelerometer biases and scale factor errors. While UWB radio technology is recognized as an ideal platform in indoor environments to provide accurate positioning information, it still poses a priority for the UWB-based indoor positioning system to consistently generate accurate location systems compared to the significant perpetuation of LOS multipath and NLOS proliferation [31].

Wireless infrastructure in terms of sensor nodes deployed in a specific region is eventually needed by fusion-based systems integrating wireless technologies. The numbers of needed UWB sensor nodes increase considerably to ensure that at least four UWB anchor nodes cover every possible environment position. The indoor environment, even so, is complicated; UWB signals reflect, as result in an error of NLOS [28]. Assuming that the INS has the attributes

of full navigation and high precision of positioning in a limited time, in-depth researches on UWB/INS combined methods has been performed by many researchers [43]. Using UWB/IMU to identify UAV [25] and to perform indoor pedestrian positioning [7], [27], but it is complex to realize the tight coupling approach suggested within this paper in practice. A UWB-based indoor positioning algorithm and strengthened PDR has been suggested in [28], but this fusion algorithm has the issue of blind signal area location drift error.

The cost-effectiveness of maximizing the fusion indoor positioning system (IPS) is massively enhanced by using an unscented Kalman filter (UKF) based IMU and UWB fusion strategy presented in [35], [54] whereby the UWB diversification has been used. The algorithm is capable of handling an abstract concept of UWB anchor nodes without such a minimal number. The same related research has been proposed in [3] with integrating a foot-mounted IMU and ZUPT using building heading information to combat heading drifts in Kalman filter, where the results compared with high-sensitivity GPS for a typical low-cost indoor pedestrian navigation system. A cascaded estimation architecture proposed in [4] to estimate the stepwise change of direction and position of one or optionally both feet, respectively, with state-of-the-art integration lower Kalman filter. Along with an indirect feedback EKF comprising a strap-down navigation technique and ZUPT detection approach with a 6DOF foot IMU sensor, which is suitably equipped. In [21] two potential data fusion approaches were analyzed by the multi-sensor indoor navigation system, composed of UWB and INS sensors. The methods of data fusion are incorporated, whereby it could both be justified by the step-length update (SLU). By using the stochastic cloning method, valid analysis of such measurements was represented.

A loosely/ tightly version of the navigation filter has been measured with real data performed by the IMU/UWB measurement period. In this research, a Backpack Navigator has been used for measurements, which was guided by the relative distance estimation of the UWB base stations (BSs). In a standard indoor situation, the data were obtained. Typically, like [20], [22], incorporating the results of various techniques by using filtering algorithms is described as loosely coupled fusion. On the other hand, while in [23], [24], the direct use of observational measurements for integrating is described as tightly coupled fusion. The EKF and tightly coupled fusion techniques are more appropriate for real-time applications, even with non-linear motions and contexts. Our research has chosen the EKF algorithm to incorporate PDR/IMU with the enhanced UWB positioning system. Based on the EKF, a tightly coupled process has been proposed. We implemented various UWB positioning system strategies to resolve issues, such as range error correction and least square algorithm limitation. Our major contributions of this research are as follows:

- A novel and comprehensive indoor pedestrian navigation and positioning solution are proposed using an improved tightly-coupled navigation model with the

combination of UWB ranging and IMU, based on the EKF algorithm.

- A TWR method for solving the pedestrian's clock drift and time synchronization issues to make the positioning results easier and more consistent to decrease positioning data's latency.
- Moreover, a real-time ranging error compensation model based on the LS method and AKF positioning algorithm is used to fix such problems, i.e., the attitude estimation in dynamic conditions. Similarly, an improved tightly coupling comparison with loosely coupling has been performed and simulated for pedestrian positioning accuracy and improvement.

The remainder of the paper is organized as Section II presents the indoor positioning and navigation of the UWB and IMU integration. Section III describes the extended Kalman filter realization as per the pedestrian. The experimental implementation, simulations and results are presented and discussed in Section IV. Section V concludes the paper with future scope.

## II. UWB AND IMU INTEGRATION IN INDOOR POSITIONING AND NAVIGATION

This section initially illustrates the indoor positioning and navigation layout with the integration of IMU and UWB-based technology, as shown in Fig. 1. The IMU sensor has a three-axis accelerometer and gyroscope. Apart from that, UWB-sensors incorporates an unknown position tag and four anchors with known positions.

*Tightly and loosely coupled integration:* A tightly coupling approach determines the positions and orientation of moving objects in dynamic indoor environments. The time difference of arrival (TDOA) method utilizes for the clock error elimination. It synchronizes the inertial sensor errors incorporating UWB ranging data fusion to correct the position. For a rigorous implementation, tight coupling and integrity monitoring are the important features for sensors data fusion. Upon this technology, a realistic IPN has been performed iteratively without any deterioration [27]. These are particularly helpful for measurements of UWB ranging, in which the outliers are common because of the effects of multipath signals refraction in NLOS situations. Furthermore, the inertial data provides accurate and consistent estimations for the UWB measurements, which provides for enhanced outliers detection. As a result, a system with a tight coupling is more stable [13]. The navigation position obtained from the UWB systems is used as measurements in an EKF, which usually corrects the drift of an INS system. In [15], [16], the pseudo ranges from UWB are used as measurements in an INS indoors. Due to the poor quality of indoor measurements, global navigation satellite system (GNSS) measurements are not usually used directly in indoor scenarios. However, satellites' measurements can provide information before and after entering buildings, establishing a starting point (and possibly orientation) in the estimation, so they could be considered decoupled measurements.

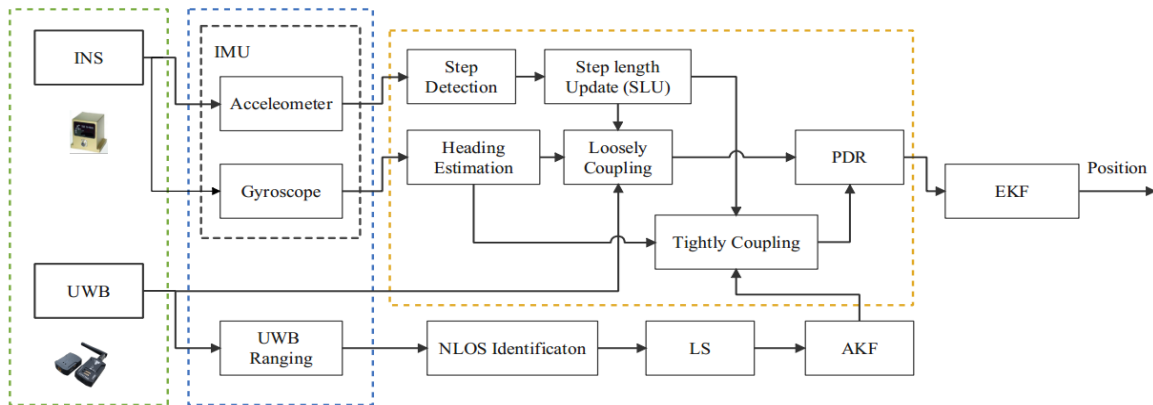


FIGURE 1. Overview of the proposed fusion algorithm.

The loosely coupling approach refers to a system in which the data from one or more independent sensors is pre-processed before it can be used to calculate the optimum results. The position estimated by this is used to initialize the UWB received signal correlators from the anchor nodes. If enough measurements are not received to estimate the position based on anchors, the INS cannot provide such information. This technique is used in [13], [14] to improve UWB estimates with inertial measurements. To increase the process of data fusion validity, a decision-making algorithm is designed. Based on a random forest algorithm and channel impulse response (CIR) data, such an algorithm evaluated the reliability of the UWB measurements. It fused all data when the UWB rangings were in LOS [20]. The measures can be used in a PDR estimation with a smooth integration scheme if the position measures are entered as position observations with a constant (and high) covariance [17]. Additionally, we suppose the system is capable of providing the covariance matrix of the position estimate. In that case, these measurements can be entered into an estimate either using step length estimates [18] or INS with ZUPT [19]. Moreover, such an approach was selected to integrate UWB ranging and INS sensors into a unified platform [47]. In [53], the pedestrian has carried a UWB sensor in his hands to avoid near floor barriers to increase the anchors' node penetration. Meanwhile, the shoe-mounted IMU could be modified to frequently resetting the drift of INS and the velocity of the ankle using the stance phases.

#### A. INS-BASED STATE PROPAGATION

The tactical and navigation IMUs would maintain position and orientation long enough, but one person cannot easily use them due to their cost, weight, and volume. Due to size and cost requirements, the only IMUs available are of the MEMS type, but due to their noise level and bias variability, they can only estimate the position accurately for a few seconds. The angle measures can triangulate for the position calculation when a measure of a person's displacements is available. It is possible to use a strong integration of the measures, improving the estimation and using measurements

even when there are not enough to achieve a position. In [8], proposed to use the measures of the length and change of angle of the PDR steps to propagate the estimate in an EKF and subsequently correct the estimates according to multiple measures received, including the angle of incidence obtained from a Ubisense's UWB system [9].

Jiménez *et al.* [10] proposed to place fiducial markers in the IMU carried by a person so that a system of cameras with known positions can measure the person's angles to be located. These angles of incidence are used as measurements in a Kalman filter propagated with the IMU measurements. Long *et al.* [11] proposed a method to correct the orientation using the magnetic field. The horizontal plane's orientation is measured during the stance stage to correct the gyroscope bias in an EKF. This approach allows the use of the magnetic field, but as in [12], they are affected by magnetic disturbances generated by metallic structures, motors, etc. The magnetic field's projection in the horizontal plane is used to estimate the orientation errors to the inertial system. If these are not detected as disturbances, they are corrected using the EKF of a PDR based on INS [11]. Ashraf *et al.* [57] proposed a magnetic pattern (MP) with convolutional neural networks (CNNs) by performing indoor localization. The database is built using MP that happens at the measuring points, and the position is determined through CNN, which compares the user-collected MP to the database. The visual-inertial EKF technique has been presented in [29] for the full filter state entirely in robocentric terms. Extrinsic camera biases, as well as additive IMU biases, are also calculated. The relative navigation principles are used to reset the step keyframe to enforce the consistency and observability of the usually heading states and unobservable position while significantly improving these features' estimation accuracy and consistency [30].

#### B. UWB SENSOR POSITIONING PROCESSING ALGORITHM

Generally, wireless signal-based positioning techniques are classified into range-based and non-range-based techniques [43]. Typically, the UWB based positioning approach incorporates the ranging algorithm with these phases.

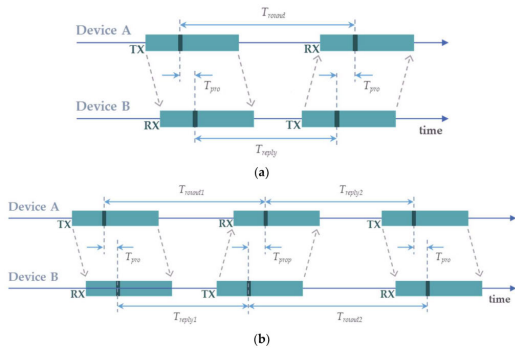


FIGURE 2. (a) and (b) shows the SDS-TWR ranging system.

The first phase is to estimate the position and angular data, and the second phase is to use the measurement position and angular data to determine the location. The widely used approach for measuring the distance between two-node is the TOF range. The UWB positioning platform is the MAX2000/DWM1000 ranging chip developed by Ireland’s DECAWAVE company. DWM1000 is a system on a chip (SoC) system solution, ranging accuracy within 30cm, has the advantages of small size, low cost, anti-multipath interference, etc. In terms of hardware implementation, the solution uses the TOF method to measure electromagnetic waves’ flight time in the medium. The specific process is a TWR method; i.e., the anchor (anchor node) and the tag (target) are not performed. Time synchronization relies on the recorded signal transmission and arrival timestamps in the two-hand handshake signal to measure electromagnetic waves’ flight time. The symmetric double-sided two-way range (SDS-TWR) system [36] is adopted mostly by recent researches in TOF to minimize the effect of the synchronization of clocks among nodes, as seen in Fig. 2. Simultaneously, it is not possible to solve the frequency drift induced either by crystal clock drift. The SDS-TWR system, in addition, takes a longer process time. We suggest a novel SDS-TWR optimization algorithm in our method to rectify the problem. Due to its highly reliable results on clock-drift error reduction when response times are symmetric, this is the most identified TWR approach in the literature.

In (1), TOF represented as  $T_{pro}$  between device A and B, from device A as  $T_{round1}$  represented the duration of time to send the polling message to receive the reply message at the same way from device B as  $T_{round2}$  represented the time is to send the reply message to obtain the final message from device A. From devices A and B, similarly,  $T_{reply1}$  and  $T_{reply2}$  are the delays of time.

$$\begin{cases} T_{round1} = 2T_{pro} + 2T_{reply2} \\ T_{round2} = 2T_{pro} + 2T_{reply1} \end{cases} \quad (1)$$

hence, between devices A and device B, TOF would be obtained as per (2),

$$T_{pro} = \frac{T_{round1} \times T_{round2} - T_{reply1} \times T_{reply2}}{T_{round1} + T_{round2} + T_{reply1} + T_{reply2}} \quad (2)$$

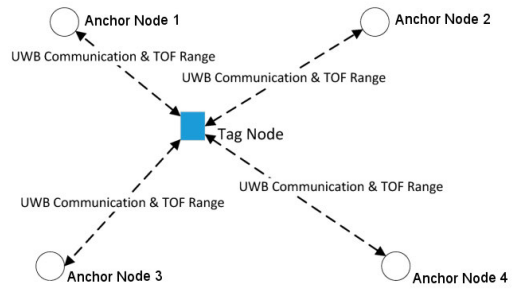


FIGURE 3. Positioning algorithm of four-UWB anchor nodes.

hence, distance ( $d$ ) can be represented as per (3),

$$d = vT_{pro} \quad (3)$$

where  $v$  represents the propagation velocity of the electromagnetic wave.

We follow the multi-lateration since performing the range phase to decide the tag location through the distance measurements. In detail, the trilateration overview is demonstrated, as seen in Fig. 3, where the distances from the tag to four-UWB-nodes have been estimated. Certainly, the tag must be placed at the four-circles intersection centred on four-UWB-nodes in the 2-dimensional plane. The trilateration consequence is unique, and know that the four-UWB-nodes aren’t really in a single direction.

Suppose an unknown tag is placed at  $(a, b)$  and  $i^{th}$  UWB-anchor node is placed at  $(a_i, b_i)$ . In (4) the accurate difference in between the  $i^{th}$  UWB-anchor node as well as the unknown tag  $d_i$  could then be defined as,

$$d_i = \sqrt{(a_i - a)^2 + (b_i - b)^2} \quad (4)$$

Assume, the measured distance represented by  $d'_i$  in between the  $i^{th}$  UWB-anchor node of the unknown tag. The variance seen between accurate distance as well as the estimated distance can be defined here as  $(p_i = d_i - d'_i)$ . In terms of dealing with its spectrum of noise, the weighted adaptive Kalman filtering approach is used to reduce the  $N$  value. In particular, each distance specifies a function of an unknown tag position as presented in (5) and (6).

$$\begin{cases} d_1^2 = (a_1 - a)^2 + (b_1 - b)^2 \\ d_2^2 = (a_2 - a)^2 + (b_2 - b)^2 \\ d_n^2 = (a_n - a)^2 + (b_n - b)^2 \end{cases} \quad (5)$$

where,

$$X = \begin{bmatrix} a_2 - a_1 & b_2 - b_1 \\ a_3 - a_1 & b_3 - b_1 \\ \vdots & \vdots \\ a_n - a_1 & b_n - b_1 \end{bmatrix}, \quad \varepsilon = \begin{bmatrix} a \\ b \end{bmatrix} \quad (6)$$

$$y = \begin{bmatrix} a_2^2 + b_2^2 - d_2^2 - (a_1^2 + b_1^2 - d_1^2) \\ a_3^2 + b_3^2 - d_3^2 - (a_1^2 + b_1^2 - d_1^2) \\ \vdots \\ a_n^2 + b_n^2 - d_n^2 - (a_1^2 + b_1^2 - d_1^2) \end{bmatrix} \quad (7)$$

Let the (7) be subtracted by (6), after all we will achieve (8).

$$X\varepsilon = y \tag{8}$$

thus, (9) shows the filtering positioning algorithm result of the  $\varepsilon$ ,

$$\varepsilon = (X^T X)^{-1} X^T y \tag{9}$$

In the filtering positioning technique, a certain weight is incorporated for each range value. Certainly, the ranging error is lower throughout the ranging phase whenever the carrier is closest to the UWB anchor node. Thus, for the lower ranging value, we select a greater weight; in this case, the positioning accuracy will be even further enhanced. To that end, we suggest a weighted adaptive Kalman filtering algorithm to address and fix the problem. The inverse of the range value “ $d$ ” is represented as the weighting coefficient  $\lambda$  as seen in (10).

$$\lambda = \begin{bmatrix} \frac{1}{d_1} & 0 & 0 & 0 \\ 0 & \frac{1}{d_2} & 0 & 0 \\ 0 & 0 & \ddots & 0 \\ 0 & 0 & 0 & \frac{1}{d_n} \end{bmatrix} \tag{10}$$

Then, the weighted adaptive Kalman filtering algorithm result of  $\hat{\varepsilon}$  is defined as in (11),

$$\hat{\varepsilon} = (X^T \lambda X)^{-1} X^T \lambda y \tag{11}$$

**C. IMU SENSOR POSITIONING PROCESSING ALGORITHM**

Fan et al. [37] performed research on the transformation of various coordinates and the estimation of the attitude function change in INS. The main principles, such as the coordination of complex models, and associated function analysis of the coordinate transformation are mainly discussed in this paper.

The integrated positioning model effectively solves the NLOS interference or occlusion interference in indoor positioning. When the anchor and card pseudo-range measurements have NLOS errors, the combined positioning model will switch the positioning solution to the INS in time and switch to the combined model after the NLOS interference disappears. Therefore, the integrated positioning system has high accuracy, good stability, and strong environmental adaptability—the integrated positioning process of the inertial navigation as seen in Fig. 4.

The black axis in Fig. 4. represents the mainline of the integrated positioning model, which realizes SIN, real-time pose shifting, 3-axis position output, speed and attitude. The purple axis represents the correction solution, which realizes Sage-Husa adaptive filtering and NLOS discrimination etc., and gives the error amount of the current state of the system [49]. The red axis represents the filter feedback, and the error amount of the measurement update solution fed back to the system state. It can be concluded from the positioning effect that the combined positioning model based on the graph optimization model can effectively estimate the heading information of pedestrian movement. The UWB ranging

value provides new constraints on the pedestrian walking trajectory. Such constraints are easy to adjust the pedestrian walking trajectory to the optimal state. A visual understanding is that the shallow coupling combination model can rotate and move the PDR trajectory to match a more realistic trajectory.

**D. ADAPTIVE KALMAN FILTER ESTIMATION IN NLOS**

In a complex indoor environment, the probability and statistical characteristics of noise are not static. E.g., the IMU is susceptible to temperature changes, and the measured value is offset; UWB ranging has multipath interference errors in some environments [48], [20]. Although it is impossible to accurately model this kind of random noise, an effective and feasible way is to appropriately adjust the mean and variance of the noise to make the white noise approximated by the model closer to the real situation. The AKF estimation algorithm identifies the mean and variance of noise online to adapt to the complex and changeable noise characteristics. Generally, the amplitude of the inertial data noise of the IMU changes slowly. The adaptive estimation only considers the mean and variance of the observed noise online to simplify the calculation process [12].

The innovation sequence of the filter is equal to the difference between a priori measurement estimate and the posterior sensor measurement. To a certain extent, the innovation value reflects the performance of AKF estimation, so Sage-Husa adaptive estimation uses this feature to identify process and measurement noises [49]. Let  $r$  be the measured noise’s deviation value; then the noises characteristic identifies as (12).

$$\begin{cases} r_{k+1} = (1-d_{k+1})r_k + d_{k+1}(\delta z_k - h(\delta x_k^-)) \\ R_{k+1} = (1-d_{k+1})R_k + d_k(\xi_{k+1}\xi_{k+1}^T - H_{k+1}P_{k+1}^- P_{k+1}^-, H_{k+1}^T) \end{cases} \tag{12}$$

where  $d_{k+1} = \frac{1-b}{1-b^{k+1}}$  represents the weight of the current residual,  $b$  is the attenuation factor. The mean value  $r_{k+1}$  and variance  $R_{k+1}$  of the measurement noise are estimated as the residual historical sequence  $(r_1, r_2 \dots R_k)$  and the new residual weighting. The residual historical information will increase with time and contribute less and less to the identification algorithm (13).

$$\begin{cases} \xi_{k+1} = Z_{k+1} - H_{k+1}X_{k+1}^- - r_{k+1} \\ K_{k+1} = P_{k+1}^-, H_{k+1}^T (H_{k+1}P_{k+1}^-, H_{k+1}^T + R_{k+1})^{-1} \end{cases} \tag{13}$$

Sage-Husa AKF estimation is a sub-optimal estimator. It uses the autocorrelation characteristics of the residual sequence to make online statistics of the mean and variance of the system noise. It has good results in practical applications.

**1) PROCESSING OF NLOS**

There is a very significant jitter error in the UWB positioning system, i.e., the NLOS error, as seen in Fig. 5. The NLOS error is closely related to the current environment. When obstacles in the linear path of the transmission signal or the

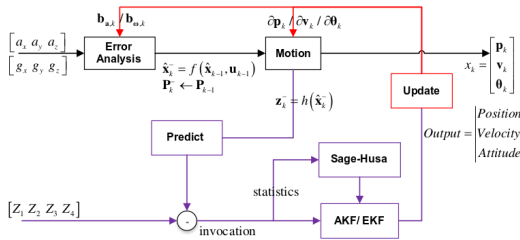


FIGURE 4. A conceptual model of inertial navigation process.

multipath effect are obvious, the range finding value is likely to be extremely inaccurate [13]. The fundamental reason for the inaccurate ranging is that the UWB hardware accepts multipath electromagnetic signals and recognizes the first signal as a straight signal without delay. This mechanism performs well for most LOS conditions. Compared with the straight signal, the signal power on the NLOS path in the received signal attenuates more. Therefore, this feature can be used to judge the error detection of the UWB hardware straight signal, which has a certain validity. The specific method of NLOS judgment is represented as (14).

$$dB = fP - rxP = \begin{cases} < TH\_1 & (LOS) \\ \geq TH\_2 & (NLOS) \end{cases} \quad (14)$$

where  $fP$  represents the power of the first path of the wireless signal received by UWB,  $rxP$  represents the total power of the wireless signal received by UWB, and  $dB$  represents the signal gain, i.e., the power ratio of the first path to the total power of the wireless signal. When the  $dB$  value is small, it indicates that the total power of the wireless signal is mainly concentrated on the first path, and the ranging quality is good; on the contrary, the power of the signal is scattered on each path, and the ranging quality is poor, which is most likely to be an NLOS situation. In addition, the tightly coupled integrated navigation model provides a probabilistic consistency test for the rationality of the data. In the EKF, the innovation is an orthogonal, time uncorrelated, white noise sequence and normalized Gaussian noise.

The target's specific coordinates could be achieved if the threshold is located and the UWB anchors are in LOS. The residual is very minimal at this point. The hyperbolic planes of TDOA can converge in a region because of the NLOS channels between the target and the UWB/IMU sensors on PDR. The target's location is unknown at this time. The residual would, of course, be incredibly large. As a result, the residual threshold could be used to decide whether an NLOS situation exists.

### III. REALIZATION ON EXTENDED KALMAN FILTER

There are mainly two techniques when applying the Kalman filter to non-linear problems for the data fusion in UWB/IMU tightly coupled positioning and navigation. The first consists of using a first-order Taylor series around a static reference path, resulting in what is known as a linearized Kalman filter [31]. It is a useful technique when there is a large amount of a priori information about the problem, such as in

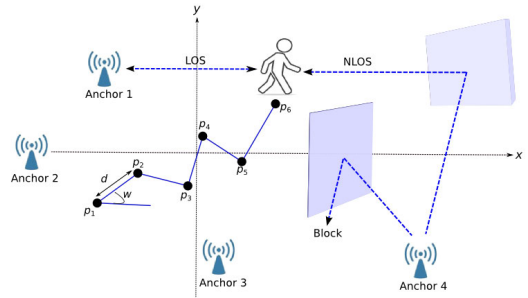


FIGURE 5. A schematic layout of signal NLOS error source.

satellite tracking, since the approximate orbit of the satellite is known in advance. The main problem with this approach is that the same reference path is used for the estimation process duration. The errors will grow without a limit if there is a large difference between the system's state and the reference path. To avoid such a problem, the solution is to linearize using a Taylor series around a dynamic reference trajectory continuously updated with state estimates that are products of the observations. Each time a new state estimate is calculated, a new, better, and more accurate reference path is recalculated and incorporated into the estimation process. When a first-order Taylor series is used, the resulting filter is known as the EKF [31], while if a second-order Taylor series is used, the second-order EKF is obtained [32]. In this work, the standard or first-order EKF will be used exclusively, based on the assumption of a non-linear system model and a non-linear observation model; the equations are described below. In the EKF, the system has to be represented by a non-linear equation of the form (15).

$$\begin{cases} x_{k-1} = f(x_k, u_k) + v_k \\ v_k \approx N(0, Q_k) \end{cases} \quad (15)$$

where  $f(\cdot)$  is a non-linear transition function, and  $v_k$  represents a Gaussian white noise disturbance, with mean  $E[v(k)] = 0$  and covariance  $Q_k$ , fulfilling that  $E[v_k(i)v_k^T(j)] = \delta_{ij}Q_k(i)$ .

As in the system model, the model that relates the observations to the state is also expressed by a non-linear equation (16).

$$\begin{cases} z_k = h(x_k) + w_k \\ w_k \approx N(0, R_k) \end{cases} \quad (16)$$

where  $h(\cdot)$  is a non-linear observation function, and  $w_k$  is a Gaussian white noise disturbance, with mean  $E[w(k)] = 0$  and covariance  $R_k$ , fulfilling that  $E[w_k(i)w_k^T(j)] = \delta_{ij}R_k(i)$ .

Similar to the linear Kalman filter, the EKF algorithm is based on a prediction-correction cycle, with the difference that a first-order Taylor series linearize non-linear functions. The equations are shown below without their mathematical development. The interested reader can find various proofs in [33], [34] among others.

*Prediction:* Given the state estimation of the system and its covariance matrix  $\hat{x}_{k|k}, P_{k|k}$  at time  $k$ , the prediction

$\hat{x}_{k+1|k}, P_{k+1|k}$  at time  $k + 1$  is calculated as per (17) and (18).

$$\hat{x}_{k+1|k} = f(\hat{x}_{k|k}, u_k) \quad (17)$$

$$P_{k+1|k} = \nabla_x f \cdot P_{k|k} \cdot \nabla_x f^T + Q_k \quad (18)$$

where the Jacobian of the state transition function  $\nabla_x f$  evaluated in the state  $x = \hat{x}_{k|k}$  is defined as (19).

$$\nabla_x f = \frac{\partial f}{\partial x} \Big|_{x=\hat{x}_{k|k}} = \begin{bmatrix} \frac{\partial f_1}{\partial x_1} & \cdots & \frac{\partial f_1}{\partial x_n} \\ \vdots & \ddots & \vdots \\ \frac{\partial f_n}{\partial x_1} & \cdots & \frac{\partial f_n}{\partial x_n} \end{bmatrix}_{x=\hat{x}_{k|k}} \quad (19)$$

*Correction:* At the instant of time  $k + 1$ , the observation  $z_{k+1}$  is carried out, and using the prediction of the state calculated in the previous phase, the estimate of the state is corrected according to the (20) and (21).

$$\hat{x}_{k+1|k+1} = \hat{x}_{k+1|k} + K_{|k+1} \cdot \tilde{z}_{k+1} \quad (20)$$

$$P_{k+1|k+1} = [I - K_{k+1} \cdot \nabla_x h] P_{k+1|k} \quad (21)$$

where (20) is the correction for the state estimate, and (19) is the correction for the state covariance, and the terms.

$$\tilde{z}_{k+1} = z_{k+1} - h(\hat{x}_{k+1|k+1}) \quad (22)$$

$$S_{k+1} = \nabla_x h \cdot P_{k+1|k} \cdot \nabla_x h^T + R_{k+1} \quad (23)$$

$$K_{k+1} = P_{k+1|k} \cdot \nabla_x h^T \cdot S_{k+1}^{-1} \quad (24)$$

where (22) represent the innovation, (23) the innovation covariance, (24) the suboptimal (or quasi-optimal) Kalman gain, and the observation function is linearized by the Jacobian  $\nabla_x h$  as (25), evaluated using the last prediction of the state  $x = \hat{x}_{k+1|k}$ .

$$\nabla_x h = \frac{\partial h}{\partial x} \Big|_{x=\hat{x}_{k+1|k}} = \begin{bmatrix} \frac{\partial h_1}{\partial x_1} & \cdots & \frac{\partial h_1}{\partial x_n} \\ \vdots & \ddots & \vdots \\ \frac{\partial h_n}{\partial x_1} & \cdots & \frac{\partial h_n}{\partial x_n} \end{bmatrix}_{x=\hat{x}_{k+1|k}} \quad (25)$$

## A. SENSOR MODEL

### 1) MOTION AND INERTIAL SENSOR DATA

The inertial sensor's error model adopts the first-order Markov noise model, and the noise of the inertial element includes Gaussian white noise and Gauss-Markov noise, as seen in (26).

$$\begin{cases} \tilde{f}_k = \tilde{f}_{k-1} b_{f,k} + Gauss(0, \sigma_f) \\ b_{f,k} = e^{-\beta \Delta T} b_{f,k-1} + Gauss(0, \sigma_{bf}) \end{cases}, \quad (26)$$

Among them  $\tilde{f}_k, \tilde{f}_{k-1}, b_{f,k}$  respectively represent the 3-axis ideal, measurement, and zero-drift specific force values of the accelerometer's sensing target,  $\Delta T$  is the sampling period,  $T_a = 1/\beta$  is the correlation time of the first-order Markov process ( $\sigma_f, \sigma_{bf}$ ). They are the zero drift uncertainty of the accelerometer and the Gaussian-Markov noise driving variance [41]. Similarly, the model of a gyroscope is similar to

that of an accelerometer. Checked the relevant MEMS-IMU sensor data manual, and configured the performance parameters of the low-cost inertial element as seen in Table. 1.

### 2) UWB POSITIONING MEASUREMENT

The measurement equation of the UWB ranging system is expressed as (27).

$$\tilde{R} = \| X_l - X_{bs} \| + v \quad (27)$$

where  $X_{bs}$  represents the space coordinate system of the UWB BS, which needs to be calibrated in advance,  $v$  is the pseudo-range error amount, which is Gaussian white noise, and  $\tilde{R}$  represents the pseudo-range value between the UWB card and the UWB BS. The accuracy of pseudo-range value measurement dramatically determines the overall positioning accuracy of the system. When the UWB measurement error is too large, it is easy to cause problems such as inaccurate positioning. In NLOS, the (28) is the noise of UWB ranging  $\tilde{f}_k$  is modeled as a white noise model and the pseudo-range value.

$$\tilde{r} = r + v, \quad (28)$$

where (29) represents Gaussian noise with a mean value of zero and a standard deviation of  $0.1m$ . For the NLOS situation in the scene, this paper makes the following assumptions.

a) Set UWB ranging at time  $t$ : The probability of NLOS error is  $p(NLOS | t) \sim U(t)$  uniformly distributed, which means that the probability of NLOS in the scene at each moment is equal.

b) Suppose that the UWB pseudo-range at time  $t$  has a NLOS error, then the amount of error  $e_{NLOS}$  obeys the bi-modal Gaussian distribution, the amount of error caused by NLOS is around  $0.4$  or  $0.8m$ . Therefore, the pseudo-range measurement value after mixing the NLOS error.

$$\tilde{r} = r + v + e_{NLOS}, \quad (29)$$

## B. SYNCHRONIZATION OF THE IMU AND UWB SIGNALS PROCESSING

For the built-in sensor system, the synchronised information collection and analysis of the two sensing modules are important. The UWB obtains the distributed information when the sensor system detects a motion. It is possible to measure the angular velocity and acceleration of the IMU to achieve the displacement and attitude through the DS-TWR technique [39]. Similarly, some variations from the actual value of the displacement are measured while using two sensors; therefore, we mitigate the optimum estimate of the position through the EKF. As parameters for the sensor, the sensors' calculated values have been used for the EKF to select the feasible closest real value. Ultimately, the optimum location estimation and attitude variance of the present time are retrieved for the sensor system. The conceptual model as presented in Fig. 6.



TABLE 1. IMU parameter configuration table in the simulation experiment.

Low-cost MEMS-IMU parameter configuration	size	unit
Accelerometer static zero drift $b_{f,0}$	[15 15 18]	mg
Accelerometer first-order Markov process correlation time $T_a$	[15 15 18]	s
Acceleration measurement noise $\sigma_f$	$[2.15\ 2.15\ 3.08] \times 10^{-2}$	$m/s^2/\sqrt{Hz}$
Accelerometer zero drift uncertainty $\sigma_{b,f}$	$[4.7\ 4.8\ 6.8] \times 10^{-6}$	$m/s^3/\sqrt{Hz}$
Gyro static zero drift $b_{\omega,0}$	[5 5 8]	deg/h
Gyro first-order Markov process correlation time $T_g$	[360]	s
Gyroscope quantization noise $\sigma_w$	$[7.6\ 7.5\ 7.6] \times 10^{-3}$	$deg/s/\sqrt{Hz}$
Gyroscope zero drift uncertainty $\sigma_{b,w}$	$[8.4\ 8.4\ 8.5] \times 10^{-7}$	$deg/s^2/\sqrt{Hz}$

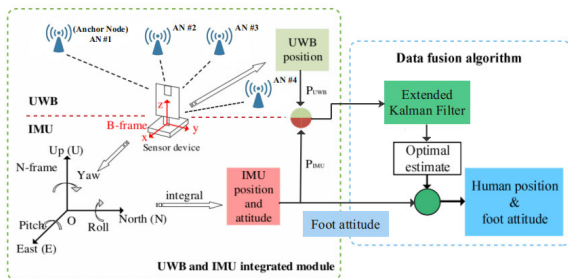


FIGURE 6. Synchronization of the IMU and UWB Signals processing.

C. PEDESTRIAN TRACK ESTIMATION SYSTEM

To reduce the inertial system’s position integration error, some researchers have proposed an INS based on gait detection called the pedestrian track estimation system. The walking movement’s characteristic is that the pedestrian’s feet repeatedly accelerate and decelerate relative to the ground, manifested as a periodic zero-crossing point of the speed [38]. Therefore, the accurate determination of pedestrian stance 3 provides the speed observation value for the inertial system, significantly improving the inertial navigation positioning accuracy.

Pedestrian track estimation system is also called step-and-heading system (SHS). There are four key steps to realize the SHS system: gait detection, step/stride length estimation, heading angle estimation, and two-dimensional position calculation [26]. Gait detection refers to using historical data of inertial elements to determine whether a pedestrian is in a stance state. The trajectory and law of the pedestrian’s footsteps during walking as seen in Fig. 7(a). The angular rate as simulated in Fig. 7(b), to ensure gait detection accuracy, the typical SHS system requires the inertial measurement unit to be mounted on shoes or legs and make the inertial measurement unit consistent with the pedestrian course.

Step/stride estimation and heading angle estimation provide the SHS system with step length and step direction data, practically the same as pure INS system. Both are equal to a single integral of inertial data. Finally, the two-dimensional position calculation superimposes the above-segmented gait geometry to form a pedestrian walking trajectory section. The SHS system itself is a potential INS. The difference is that it

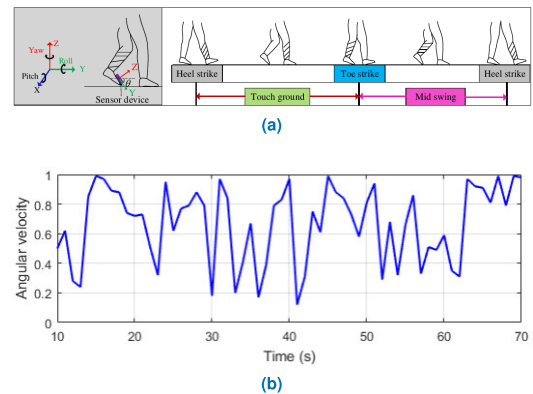


FIGURE 7. (a) Pedestrian gait posture.(b) Angular rate.

uses gait detection technology to segment (divide) INS data and output gait data, summarising the system into a series of (step length, heading) pairs [40]. Therefore, the SHS system still suffers from cumulative errors. For long-term navigation services, other information needs to be integrated for global correction.

1) GAIT DETECTION

The primary task of SHS is the recognition of steps or strides in motion data. A stable algorithm must ensure accurate step detection. There are currently two main types of algorithms.

- 1) Stance detection algorithm (Stance detection), to identify the cycle of a foot on the floor. The sensor is installed on the feet of pedestrians. Generally, these algorithms are suitable for measuring the number of steps, but the effect of step segmentation between step and step in motion data is very poor.
- 2) Step cycle detection algorithm (Step cycle detection), which detects the cycle of sensor data caused by repeated motion during walking, involves searching for repetitive patterns or repetitive motion data events (such as pedestrian heels repeatedly leaving and touching the ground). These algorithms are very suitable for step segmentation [26].

The typical stance detection algorithm is based on the idea of the threshold. The principle is that during the standing period when the foot touches the ground, the sensor is stationary,

the inertial sensor detects the pedestrian movement is not large. The threshold is set to recognize this posture easily. A successful stance detection assumes that each step's foot is a gait of walking, and the pedestrian stance discrimination model is expressed as per the mathematical equation (30).

$$Z(\{s_{\tilde{f}_k}, s_{\tilde{w}_k}\}_{w_k}) < \gamma_z \quad (30)$$

where  $Z(\cdot)$  is the zero-rate verification function in the statistical sense  $\{s_{\tilde{f}_k}, s_{\tilde{w}_k}\}_{w_k}$ , is the inertial measurement unit's sensor data in the window  $w_k$  and  $\gamma_z$  is the zero-rate detection threshold. Certainly, the zero rate value implied here can be used as a pseudo-measurement value of the observation equation, namely represented as (31),

$$\tilde{z}_k = \tilde{v}_k \forall k : Z(\{s_{\tilde{f}_k}, s_{\tilde{w}_k}\}_{w_k}) < \gamma_z \quad (31)$$

## 2) GAIT STEP-LENGTH ESTIMATION

Basically, the SHS system is also a kind of INS system, so the system motion equation is expressed as (32),

$$\begin{bmatrix} n_{p_k} \\ n_{v_{k+1}} \\ q_{k+1} \\ \delta_{f,k+1} \\ \delta_{\omega,k+1} \end{bmatrix} = \begin{bmatrix} I & I\Delta T^2 & \dots & -R\Delta T^2/2 & O \\ O & I & \dots & -R\Delta T & \dots \\ \dots & \dots & \Omega(-\delta_{\omega,k}) & \dots & O \\ O & \dots & \dots & e^{-\beta_1\Delta T} & e^{-\beta_2\Delta T} \end{bmatrix} \times \begin{bmatrix} n_{p_k} \\ n_{v_k} \\ q_k \\ \delta_{f,k} \\ \delta_{\omega,k} \end{bmatrix} + \begin{bmatrix} R\Delta T^2/2 & O \\ R\Delta T & \dots \\ \dots & q_k \otimes \\ O & O \end{bmatrix} \begin{bmatrix} s_{\tilde{f}_k} \\ s_{\tilde{w}_k} \end{bmatrix} + B_k e_k \quad (32)$$

Gait detection gives the movement when the pedestrian stance appears and indirectly provides the motion state's speed observation value, so it is brought into the observation equation, and the following measurement equation can be obtained as (33).

$$\tilde{z}_k = H \begin{bmatrix} n_{p_k} \\ n_{v_k} \\ q_k \end{bmatrix} + n_k \quad (33)$$

where  $H = [O \ I_{3 \times 3} \ O]$  is the observation matrix, and  $n_k$  is the measurement noise. Therefore, according to the motion, as mentioned above model, measurement equation, and gait pseudo-measurement value to achieve the EKF, the target position, speed, and other information can be estimated. This calculation method is called the ZUPT algorithm.

However, all the error states of the Kalman filter under the ZUPT model are not completely appreciable. Ideally, when the system is at zero-velocity in a continuous period, the target has no acceleration in all directions, i.e.,  $g = q_k \otimes s_{\tilde{f}_k} q_k^*$ . It has been proved in literature [25] that the EKF is only observable for speed  $v_k$ , roll and pitch, but not for position  $p_k$  and heading angle  $\psi_k$ . If the process noise is ignored, the

covariance of the considerable state variables will decay and tend to zero within a period of time, indicating no difference between the state estimate and the true value. The filter converges to the true value. Therefore, during the pedestrian standing, the covariance matrix of the system after a certain period of zero rate correction will be approximated as (34).

$$\text{cov}(p_k, v_k, \psi_k) = \begin{bmatrix} P_{p_k} & 0_{3 \times 5} & P_{p_k, \psi_k} \\ 0_{5 \times 3} & 0_{5 \times 5} & 0_{5 \times 1} \\ P_{p_k, \psi_k}^T & 0_{1 \times 5} & P_{\psi_k} \end{bmatrix} \quad (34)$$

The accuracy of the IMU and UWB modules is assessed in this section, as shown in Fig. 8. A gait has been performed to calculate the step after the sensor device has been connected to the foot. An IMU measurement was made on the experimenter's shoes to achieve the gait distance. The displacement has been measured using the relative position of the IMU direction point as a reference point. The two modules calculate the displacement of repetitive gait events. Fig. 8(a), the black indicator (bolds) represents the two modules' measurement effects for 12 gait activities performed 12 times. The IMU moduents during gait activities are shown in Fig. 8(b). When the system detects that the stride is at zero-velocity, the velocity in the state quantity quickly converges to the correct value, and the variance is stable and tends to zero. The following conclusions are drawn from the covariance matrix (34).

The random variable position  $p_k$ , heading angle  $\psi_k$  and the random variable speed  $v_k$ ,  $[\phi_k, \theta_k]$  is not statistically relevant. Due to the first-order Markov hypothesis in the state space and the translational rotation invariance of the state equation. This means that the recurring speed  $v_k$  and  $[\phi_k, \theta_k]$  values are irrelevant to the current position  $p_k$  and heading angle  $\psi_k$ . Therefore, ZUPT cannot reduce the uncertainty (variance) of current position  $p_k$  and heading angle  $\psi_k$ . In other words, if we reset the system position  $p_k$  and heading angle  $\psi_k$  at a certain moment, after generating a new relative position and relative heading angle. Adding them to the pre-reset state value does not cause any numerical difference to the system. The reset system means that the position  $p_k$  and the heading angle  $\psi_k$  need to be set to zero. If the estimated position and heading angle are expressed as  $d_{p_l}$  and  $d_{\psi_l}$  after the  $l^{th}$  reset, the pedestrian track estimation system is based on the step length unit (35).

$$\begin{bmatrix} X_l \\ x_l \end{bmatrix} = \begin{bmatrix} X_{l-1} \\ x_{l-1} \end{bmatrix} + \begin{bmatrix} R_{l-1} d_{p_l} \\ d_{\psi_l} \end{bmatrix} + w_k \quad (35)$$

where  $X_l$  and  $x_l$  represent the three-dimensional position in the global coordinate system and the heading angle of the carrier coordinate system relative to the coordinate navigation system in the horizontal plane (36).

$$R_l = \begin{bmatrix} \cos(x_l) & -\sin(x_l) & 0 \\ \sin(x_l) & \cos(x_l) & 0 \\ 0 & 0 & 1 \end{bmatrix}, \quad (36)$$

the local coordinate system's rotation matrix relative to the coordinate navigation system when the system was the last

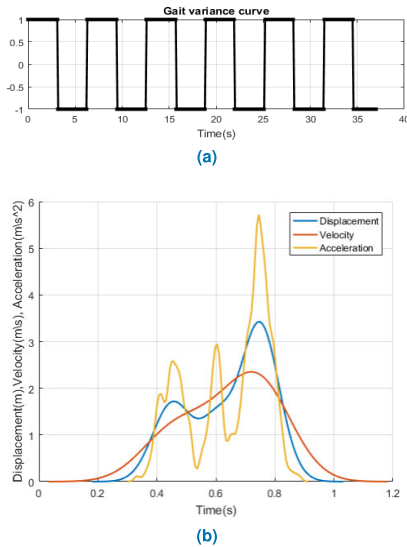


FIGURE 8. (a) Gait variance curve applying ZUPT (b) Gait displacement, velocity and acceleration.

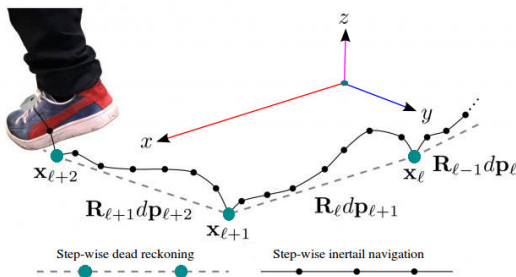


FIGURE 9. Track estimation system based on gait segmentation.

reset. The noise is assumed to be white noise, and its variance can be expressed (37).

$$\begin{aligned} cov(W_l) &= cov([R_{l-1}d_{p_l}, d_{x_l}]) \\ &= \begin{bmatrix} R_{l-1}d_{p_l}R_{l-1}^T & R_{l-1}d_{p_l},\psi_l \\ d_{p_l},\psi_l^T R_{l-1}^T & d_{\psi_l},\psi_l \end{bmatrix}, \end{aligned} \quad (37)$$

the covariance matrix  $cov(W_l)$  represents the cumulative uncertainty of the position  $p_k$  and the heading angle  $\psi_k$  since the system has been reset last time. It is also equal to the variance value of the covariance matrix converted to the coordinate navigation system.

To obtain the gait  $(d_{p_l}, d_{\psi_l})$  from the INS, it is important to select a reasonable reset time point, i.e., to segment the gait of the PDR system accurately. The condition that the gait segmentation must meet is that the EKF has converged at the time of gait segmentation, i.e., the variance of some states in formula (34) tends to zero. And there is no correlation between the position quantity  $p_k$  and the heading angle  $\psi_k$ . Obviously, the longer the standing duration, the higher the EKF's convergence, and the smaller the cross-correlation covariance in the covariance matrix. This means that gait segmentation should be performed while pedestrians are standing, as shown in Fig. 9. If the standing time is too short, the cross-correlation between the state quantities in formula (34) may not yet converge.

In short, the necessary conditions for gait segmentation are summarized as sufficiently low cross-correlation of state variables and preventing repeated resetting of the same convergence process. When this condition is established, the system applies for reset operation, and the judgment condition becomes (38).

$$(P_{v_{x_k}} < \gamma_p) \wedge (c_p < c_{min}), \quad (38)$$

where  $c_{min}$  represents the minimum sampling times between two resets. When the stance is about to end, or the application reset duration has reached the maximum, the reset operation will be executed as (39).

$$(Z(\{s_{\tilde{f}_k}, s_{\tilde{w}_k}\}_{w_k}) \geq \gamma_z) \vee (c_d > c_{max}), \quad (39)$$

Among them,  $c_{max}$  represents the maximum sampling times of continuous application for reset. Conditions in (algorithm.1, numbers 10 and 11) are indispensable in gait segmentation, and together they constitute an effective gait segmentation mechanism. After gait segmentation, the INS outputs the mileage information of pedestrian tracks. Therefore, the position calculation only needs to accumulate mileage information to obtain the target's coordinate value. The equation of motion is expressed as (40).

$$\begin{bmatrix} X_l \\ x_l \end{bmatrix} = \begin{bmatrix} X_{l-1} \\ x_{l-1} \end{bmatrix} + \begin{bmatrix} R_{l-1} & 0 \\ 0 & 1 \end{bmatrix} \begin{bmatrix} d_{p_l} \\ d_{x_l} \end{bmatrix} + w_l, \quad (40)$$

where  $X_l$  represents the 2D position of the target and  $x_l$  represents the heading angle of the target relative to the world coordinate system. The control quantity  $(d_{p_l}, d_{x_l})$  represents each step's displacement and rotation angle relative to the previous step provided by the PDR system gait segmentation. And  $w_l$  represents the cumulative error of each step is modelled as Gaussian white noise, its mean is 0, and the variance is time-varying and given by PDR.

The PDR system divides the inertial data and generates a series of (step length, heading) pairs, and the algorithm of gait segmentation is expressed as follows.

#### IV. EXPERIMENTAL IMPLEMENTATION, SIMULATIONS AND RESULTS

This paper transplants the algorithm to the embedded STM32F407 microcomputer platform as the main controller chip, as seen in Fig. 10, to realize the UWB/IMU combined positioning system based on EKF. The indoor positioning test in the actual environment is carried out in the corridor of the robotics laboratory of the School of Information Engineering, as shown in Fig. 11. The main experimental processes are; 1) where hardware configuration has a 4-UWB anchor (MAX2000/DWM1000) and a 6-axis 1 UWB/MEMS-IMU (MPU6050) card node on the top of the right foot to ensure that there are no obstructions (or obstacles) on the rectangular path of all anchors and card, 2) The experimenter walks around the prescribed rectangular path as shown in Fig. 12(a), 3) Other staff members realized the NLOS situation during the experiment, standing in front of the anchor node.

**Algorithm 1** Gait Segmentation for PDR System

---

```

1:  $k := l := cp := cd := 0$ 
2:  $p_k := v_k := 0_{3 \times 1}$ 
3:  $q_k := [\text{coarse self} - \text{initialization}]$ 
4:  $P_k := [\text{initial velocity, roll and pitch uncertainty}]$ 
5:  $(X_l, x_l) := [\text{initial position and heading}]$ 
6:  $P_{X_l, x_l} := [\text{initial position and heading uncertainty}]$ 
   loop
7:    $k := k + 1$ 
8:  $(([p_k, v_k, q_k], P_k) \leftarrow ([p_{k-1}, v_{k-1}, q_{k-1}], P_k, \tilde{f}_k, \tilde{w}_k)$ 
   //zupt - aided inertial navigation
9:    $c_p := c_p + 1$ 
10:  if  $(P_k < \gamma_p) \wedge (c_p > c_{min})$  then
11:     $c_d := c_d + 1$ 
12:  end if
13:  if  $(Z(\{s_{\tilde{f}_k}, s_{\tilde{w}_k}\}_{w_k}) \geq \gamma_z) \vee (c_d > c_{max})$  then
14:     $l := \tilde{l} + 1$ 
15:     $d_{p_l} := \bar{p}_k, d\psi_l = \bar{\phi}_k, P_{w_l}$ 
16:     $p_k := v_k := 0, \psi_k = 0$ 
17:     $P_{k[1:3,9] \times [1:3,9]} := 0_{4 \times 4}$ 
18:     $c_p := 0, c_d := 0$ 
19:     $([X_l, x_l], P_l) \leftarrow ([X_{l-1}, x_{l-1}], P_{l-1}, d_{p_l}, d\psi_l, P_{w_l})$ 
   //step - wise dead reckoning
20:  end if
21:  return loop

```

---

The UWB anchors were placed near the gait (pedestrian) trajectory, as shown in Fig. 12(a), where the key points are marked as the fixed point as P and anchors as A in 2D coordinates for measurement purposes seen in Table 2. The UWB tag and IMU have been mounted on the shoe of the experimenter. The experimental structure is rectangular because the combined positioning algorithm has been used primarily to enhance pedestrian tracking accuracy. Fig. 12(a) represented 2D which is illustrated in the experimental scene. The anchors are represented as A(1)- A(4) and P(1)- P(6) denotes the fixed point, where the experiment conductor starts at P(1) as the (starting point), then moves around P(2), P(3), P(4), P(5), and P(6) before returning to P(1), as seen by the red arrows. Before the actual test, the IMU system was adjusted and mounted on the experimenter's foot. The X-axis points to the right side of the (body), the Y-axis points to the forwards' (body), and the Z-axis point upwards. The two positioning systems' timestamp (TS) data is used to achieve time synchronization during the data-gathering phase.

### A. GAIT TRACK ON VARIOUS RECTANGULAR TRAJECTORIES

The simulation experiment scene is positioned with a length, width, and height of  $300 \times 150 \times 50\text{cm}$ , as seen in Fig. 11 and with a simulation in Fig. 12(a). The black circles represent the anchor's location, and the red triangle points represent the origin coordinates. The target movement process and target motion state undergo various states such as linear motion, circular motion, acceleration, deceleration, and uniform motion. After combined positioning and calculation, the system error accuracy is controlled within 10cm, and the speed is controlled with  $6\text{m/s}$ . The positioning system pays more attention to pedestrian location services.

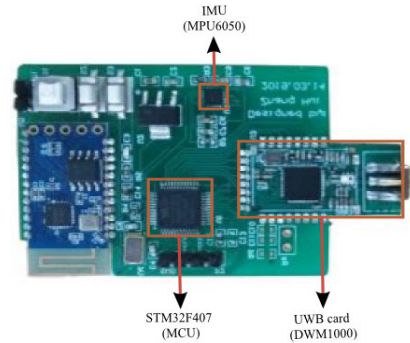


**FIGURE 10.** UWB/IMU main controller platform.

In this research, MATLAB R2016b has been used for simulation purposes. Performing the simulation to set the trajectory passing points' position and posture can automatically generate a smooth motion trajectory. Fig. 12 displays the IMU-measured position, UWB-measured position, and fusion results after moving around the trajectory once. It seems to be clear to see from the obtained results.

- 1) NLOS obstruction of the experimenter's ankle induced a bias error in the system of UWB. The positioning error affected by NLOS has been seen in the positioning outcome of UWB many times, as seen in Fig. 12(a), and the error in the top left corner was found crucial. Even though positioning accuracy improved efficiency for indoor environments applications, the outcomes have been unstable due to ambient interference from the UWB system.
- 2) As shown by the deviation between black and blue lines in Fig. 12(b), an apparent systemic error in the IMU estimation has also been challenging for the system to clarify. Therefore the present position determined by combining the previous moment's deviations in this case. Hence, the position, on the other hand, remained reasonably constant, and the errors for a single gait hasn't been significant.
- 3) The above two methods performances have been incorporated for the UWB/IMU combined system. The inertial data has been used to adjust the UWB positioning data to make it more reliable, as well as the UWB data has been used to correct for the inertial positioning. The fusion technique corrected the two-set of measurements data, resulting in more efficient and reliable final positioning results, as seen in Fig. 12(c).

The positioning effect is shown in Fig. 12; pedestrians stay on the ground, where the footsteps' trajectory curve shows the real-time pedestrian movement.

### 1) UWB RANGING AND IMU INTEGRATED POSITIONING AND COMPARISON

The indoor positioning system with UWB/MEMS-IMU integrated positioning EKF filter and UWB ranging is realized to draw the true trajectory and output of the positioning system error curve, as shown in Fig. 14. When there is an NLOS error in the ranging value, the UWB ranging system's

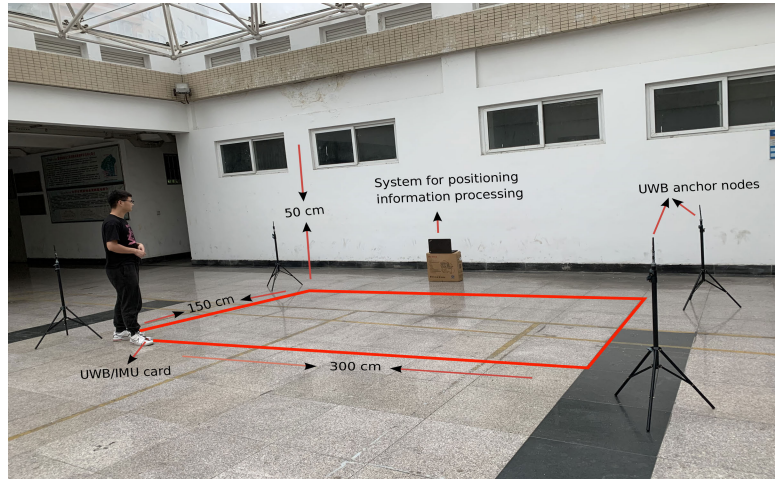
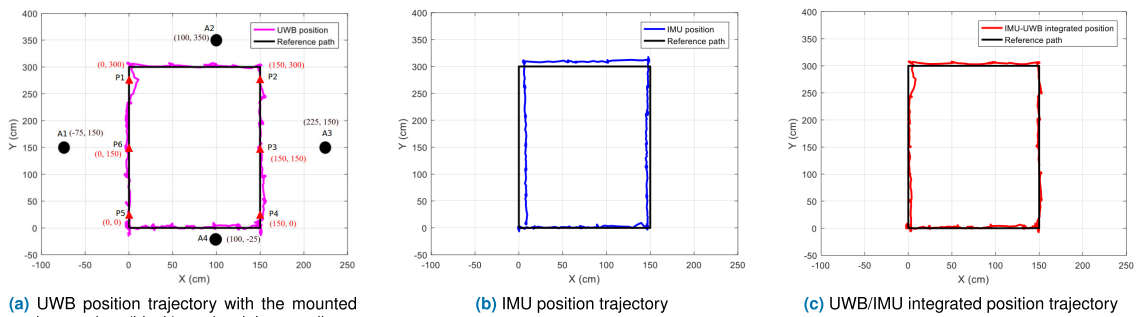


FIGURE 11. Indoor positioning experimental setup scene.



(a) UWB position trajectory with the mounted anchor nodes (black) and origin coordinate points (red).

(b) IMU position trajectory

(c) UWB/IMU integrated position trajectory

FIGURE 12. Rectangular pedestrian tracks along the estimated positions.

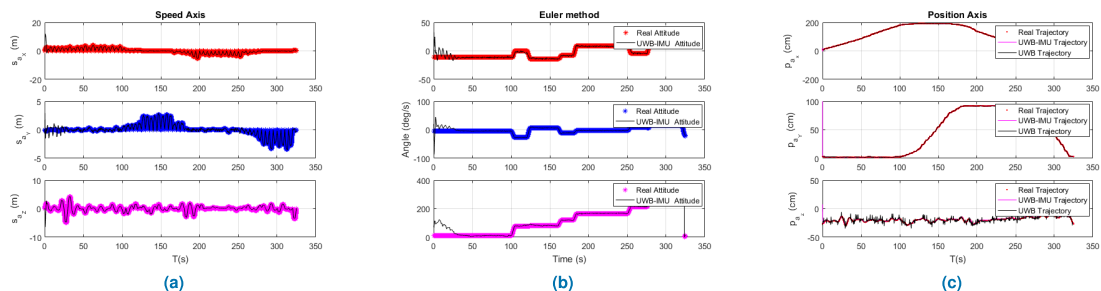


FIGURE 13. (a), (b) and (c) represent UWB/IMU combined positioning speed and attitude.

output is unstable, showing a large position jitter [42]. The combined positioning system is not affected where the error is controlled within 0.1 m—indicating that the combined positioning model based on EKF can effectively track the target’s position, which has a more significant non-linear approximation accuracy. It can quickly converge near the true value, improving the susceptibility of the UWB ranging positioning system to NLOS interference; however, the positioning system exhibits poor performance in the height direction, which verifies the conclusion of the BS layout transmission system error.

By comparing the position error curves of the accelerometer and gyroscope, as shown in Fig. 15(a) and (b), besides Fig. 13(a), (b) and (c) show the UWB/IMU combined positioning model, which can also provide accurate speed and

position information of the target’s, respectively. The EKF filter’s poor accuracy can be an NLOS error in the range, so the filter cannot recognize such a situation. The position amount is corrected to deviate from the actual value, where the new LOS pseudo-range value appears. The measurement in the update and non-linear processing link, the first-order approximation error is too large because the step size is too large, and the filter has a brief jitter. The UKF filter calculation is more significant than that of the EKF, but it’s unsuitable for some platforms with tight computing resources.

The mileage information estimated by the PDR system is very accurate in a short time. When the PDR system does not include an IMU, i.e., accelerometer and gyroscope, the PDR knows nothing about the system’s heading information. Therefore, the feasible idea is to use the ranging information

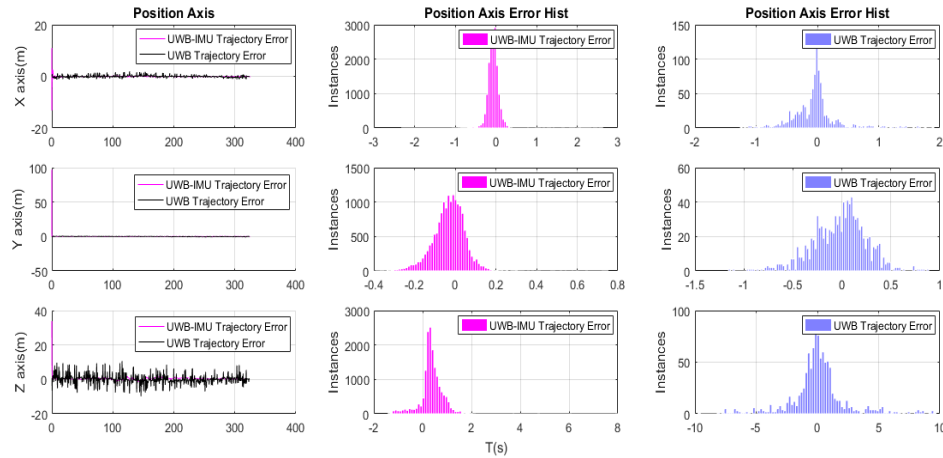


FIGURE 14. UWB/IMU combined positioning trajectories error.

provided by UWB positioning to estimate the heading angle and, at the same time, establish the distance constraint of the historical trajectory of the target to correct the divergence of the position integral to realize a positioning system with low accuracy. The PDR system assumes that the sensor is close to the foot (there is no relative movement), and the sensor speed is zero at the moment of walking and standing posture (the foot touches the ground or the foot leaves the bottom). Its application means that the integration of open-loop inertial data only occurs during the foot’s swing phase. The drift is limited for such a process with a short integration duration, so short/mid-term position tracking is feasible. However, for a reliable output system, the PDR system must be applied only when the foot (sensor) is stationary, and the sensor installed on the higher part of the foot may cause problems. From the perspective of the transition from standing to foot swing, the heel is lifted soon after the pedestrian steps down. Therefore, the sensor installed in the middle of the foot will experience upward acceleration when the foot starts to lift. Therefore, there will be some small accelerations before the end of the standing phase. The above simulation experiment successfully verified the effectiveness of the integrated navigation algorithm.

2) LOOSELY AND TIGHTLY COUPLING, AND OTHER ALGORITHMS IMPACT ON UWB/IMU

The tracking results of both loosely and tightly coupling approaches have been compared. The black trajectory shows the real tracking route during the simulation experiment, as shown in section IV (A) Fig. 12(a). At the same time, comparing the UWB/IMU integration through loosely and tightly couplings. The red curve in Fig. 16(a) represents the loosely coupling, and the blue curve represents the tight coupling during the experiment. Using the tightly coupling algorithm on UWB/IMU to estimate the pedestrian track shows more stability than the loosely coupling algorithm. The tightly coupling algorithm’s accuracy is greater and better than the loosely coupling, as seen from the figures because

TABLE 2. Key-points pedestrian trajectory and UWB anchors position coordinates (in centimeter).

UWB (anchor)	Coordinate (cm,cm)	Key (point)	Coordinate (cm,cm)
A(1)	(-75, 150)	P(1)	(0, 300)
A(2)	(100, 350)	P(2)	(150, 300)
A(3)	(225, 150)	P(3)	(150, 150)
A(4)	(100, -25)	P(4)	(150, 0)
		P(5)	(0, 0)
		P(6)	(0, 150)

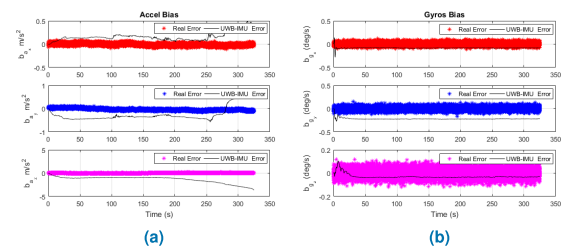
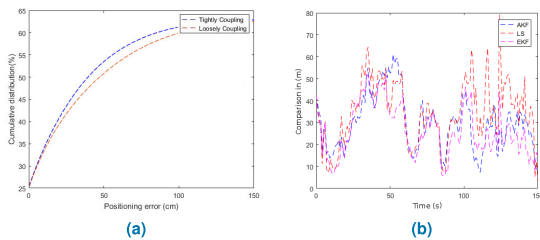


FIGURE 15. UWB ranging and IMU positioning error comparison based on (a) accel and (b) gyro biases.

it’s similar to the actual motion trajectory. As a result, the tightly coupling method’s position is more consistent and accurate when the variances are compared. The UWB system pedestrian tracking result shows a few positioning jump points because of the NLOS error during the gait process. The overall positioning error is minimized since the jump point is corrected in the tightly and loosely coupled algorithms. The tightly coupling has an estimated positioning accuracy of around 11cm, which is 53.26% better than the loosely coupling, which is 38.24% in cumulative distribution.

Moreover, the EKF fusion positioning algorithm is first compared to the AKF and LS positioning algorithms on the UWB/IMU, as shown in Fig. 16(b). In addition, the tightly and loosely coupling methods have been performed on these algorithms and compared in terms of efficiency and the positioning error compared among the LS, AKF and EKF algorithms. It means that observation noise seems to have a large effect on the measurements. The accuracy could be



**FIGURE 16. (a) Tightly and loosely comparison on pedestrian gait navigation (b) Algorithms comparison on the trajectories of integrated UWB/IMU position.**

greatly improved after using the proposed EKF algorithm on AKF and LS, and the findings are much closer to the actual trajectory, as shown in Fig. 16(b). Furthermore, it can be seen that the EKF path remains stable as the observation noise variance increases. Like the process noise variance increases, the carrier's motion becomes curvilinear, as shown in Fig. 12. The path accuracy can be greatly improved after using the proposed EKF algorithm, and the results are much closer to the actual trajectory.

## V. CONCLUSION AND FUTURE SCOPE

In this research, an indoor environment foot-mounted PDR navigation approach is proposed by integrating the IMU and UWB ranging sensor fusion to provide a generic indoor positioning accuracy solution. We applied EKF to incorporate a foot-mounted IMU in a tightly coupled fashion to a 2D pedestrian positioning solution through UWB signals by comparing the AKF and LS. Moreover, the paper considered the UWB NLOS IMU error identification during gait. A real-time ranging error compensation model of integrated IMU and UWB trajectories comparison is simulated through AKF and LS, similarly with a new tightly coupling and loosely coupling in a TWR manner for the effectiveness of pedestrian positioning accuracy and improvement. Therefore, the experiments in a dynamic indoor environment validated the efficacy of the above-proposed approaches for error minimization. Future research in the indoor environment will enhance positioning results by randomly incorporating dual foot-mounted IMU gait movement with the help of tightly coupling fusion of UWB ranging and IMU PDR in an effective and robust method.

## ABBREVIATIONS

UWB	Ultra-wideband.
IMU	Inertial measurement unit.
NLOS	Non-line-of-sight.
PDR	Pedestrian dead reckoning.
EKF	Extended Kalman filter.
AKF	Adaptive Kalman filter.
LSs	Least-squares.
INS	Inertial navigation system.
TWR	Two-way ranging.
SDS-TWR	Symmetric double-sided two-way range.
GPS	Global positioning system.
IPN	Indoor pedestrian navigation.

CoM	Center of mass.
WiFi	Wireless fidelity.
RFID	Radio-frequency identification.
MEMS	Micro-electromechanical systems.
RSSI	Signal strength indicator.
MP	Magnetic pattern.
CNN	Convolutional neural networks.
TOF	Time of flight.
KF	Kalman filter.
ZUPTs	Zero-velocity updates.
ZARUs	Zero-angular rate updates.
DOF	Degrees of freedom.
LOS	Line-of-sight.
UKF	Unscented Kalman filter.
IPS	Indoor positioning system.
SLU	Step-length update.
BSs	Base stations.
CIR	Channel impulse response.
GNSS	Global navigation satellite system.
SINS	Strap-down inertial navigation system.
TDOA	Time difference of arrival.
SHS	Step-and-heading system.
TS	Timestamp.

## ACKNOWLEDGMENT

The authors are indebted for designing and conducting the experiments by using the Robotics Laboratory of the School of Information Engineering, Southwest University of Science and Technology, Mianyang, China.

## REFERENCES

- [1] S. Iwata, K. Ishikawa, T. Takayama, M. Yanagisawa, and N. Togawa, "Robust indoor/outdoor detection method based on sparse GPS positioning information," in *Proc. IEEE 8th Int. Conf. Consum. Electron.*, Berlin, Germany, Sep. 2018, pp. 1–4, doi: [10.1109/ICCE-Berlin.2018.8576188](https://doi.org/10.1109/ICCE-Berlin.2018.8576188).
- [2] F. Pervez, J. Qadir, M. Khalil, T. Yaqoob, U. Ashraf, and S. Younis, "Wireless technologies for emergency response: A comprehensive review and some guidelines," *IEEE Access*, vol. 6, pp. 71814–71838, 2018, doi: [10.1109/ACCESS.2018.2878898](https://doi.org/10.1109/ACCESS.2018.2878898).
- [3] K. Abdulrahim, C. Hide, T. Moore, and C. Hill, "Aiding MEMS IMU with building heading for indoor pedestrian navigation," in *Proc. Ubiquitous Positioning Indoor Navigat. Location Based Service*, Kirkkonummi, Finland, Oct. 2010, pp. 1–6, doi: [10.1109/UPINLBS.2010.5653986](https://doi.org/10.1109/UPINLBS.2010.5653986).
- [4] B. Wagstaff, V. Peretroukhin, and J. Kelly, "Improving foot-mounted inertial navigation through real-time motion classification," in *Proc. Int. Conf. Indoor Position Indoor Navigat. (IPIN)*, Sapporo, Japan, 2017, pp. 1–8, doi: [10.1109/IPIN.2017.8115947](https://doi.org/10.1109/IPIN.2017.8115947).
- [5] Z. Li, G. Chang, J. Gao, J. Wang, and A. Hernandez, "GPS/UWB/MEMS-IMU tightly coupled navigation with improved robust Kalman filter," *Adv. Space Res.*, vol. 58, no. 11, pp. 2424–2434, Dec. 2016, doi: [10.1016/j.asr.2016.07.028](https://doi.org/10.1016/j.asr.2016.07.028).
- [6] G. Miraglia, K. N. Maleki, and L. R. Hook, "Comparison of two sensor data fusion methods in a tightly coupled UWB/IMU 3-D localization system," in *Proc. Int. Conf. Eng., Technol. Innov. (ICE/ITMC)*, Madeira, Portugal, Jun. 2017, pp. 611–618, doi: [10.1109/ICE.2017.8279941](https://doi.org/10.1109/ICE.2017.8279941).
- [7] Y. Li and J. Jack Wang, "A pedestrian navigation system based on low cost IMU," *J. Navigat.*, vol. 67, no. 6, pp. 929–949, Nov. 2014, doi: [10.1017/s0373463314000344](https://doi.org/10.1017/s0373463314000344).
- [8] H. A. A. Dafallah, "Design and implementation of an accurate real time GPS tracking system," in *Proc. 3rd Int. Conf. E-Technol. Netw. Develop. (ICeND)*, Apr. 2014, pp. 183–188, doi: [10.1109/icend.2014.6991376](https://doi.org/10.1109/icend.2014.6991376).

- [9] H. Hellmers, A. Norrdine, J. Blankenbach, and A. Eichhorn, "An IMU/magnetometer-based indoor positioning system using Kalman filtering," in *Proc. Int. Conf. Indoor Posit. Indoor Navig. (IPIN)*, Montbeliard, France, 2013, pp. 1–9, doi: [10.1109/IPIN.2013.6817887](https://doi.org/10.1109/IPIN.2013.6817887).
- [10] A. R. Jiménez, F. Seco, J. C. Prieto, and J. Guevara, "Indoor pedestrian navigation using an INS/EKF framework for yaw drift reduction and a foot-mounted IMU," in *Proc. Workshop Positioning, Navigat. Commun.*, Dresden, Germany, 2010, pp. 135–143, doi: [10.1109/WPNC.2010.5649300](https://doi.org/10.1109/WPNC.2010.5649300).
- [11] K. Long, C. Shen, C. Tian, K. Zhang, U. A. Bhatti, D. F. N. Kong, S. Feng, and H. Cheng, "Single UWB anchor aided PDR heading and step length correcting indoor localization system," *IEEE Access*, vol. 9, pp. 11511–11522, 2021, doi: [10.1109/ACCESS.2021.3050405](https://doi.org/10.1109/ACCESS.2021.3050405).
- [12] W. Li and J. Wang, "Effective adaptive Kalman filter for MEMS-IMU/magnetometers integrated attitude and heading reference systems," *J. Navigat.*, vol. 66, no. 1, pp. 99–113, 2013, doi: [10.1017/s0373463312000331](https://doi.org/10.1017/s0373463312000331).
- [13] X. Li, Y. Wang, and K. Khoshelham, "UWB/PDR tightly coupled navigation with robust extended Kalman filter for NLOS environments," *Mobile Inf. Syst.*, vol. 2018, pp. 1–14, Dec. 2018, doi: [10.1155/2018/8019581](https://doi.org/10.1155/2018/8019581).
- [14] J. Wang, Y. Gao, Z. K. Li, X. L. Meng, and C. M. Hancock, "A tightly-coupled GPS/INS/UWB cooperative positioning sensors system supported by V2I communication," *Sensors*, vol. 16, no. 7, p. 944, 2016, doi: [10.3390/s16070944](https://doi.org/10.3390/s16070944).
- [15] Y. Xu, T. Shen, X.-Y. Chen, L.-L. Bu, and N. Feng, "Predictive adaptive Kalman filter and its application to INS/UWB-integrated human localization with missing UWB-based measurements," *Int. J. Autom. Comput.*, vol. 16, no. 5, pp. 604–613, Oct. 2019, doi: [10.1007/s11633-018-1157-4](https://doi.org/10.1007/s11633-018-1157-4).
- [16] M. Angermann and P. Robertson, "FootSLAM: Pedestrian simultaneous localization and mapping without exteroceptive sensors—Hitchhiking on human perception and cognition," *Proc. IEEE*, vol. 100, no. 1, pp. 1840–1848, May 2012, doi: [10.1109/JPROC.2012.2189785](https://doi.org/10.1109/JPROC.2012.2189785).
- [17] A. F. G. Ferreira, D. M. A. Fernandes, A. P. Catarino, and J. L. Monteiro, "Localization and positioning systems for emergency responders: A survey," *IEEE Commun. Surveys Tuts.*, vol. 19, no. 4, pp. 2836–2870, 4th Quart., 2017, doi: [10.1109/COMST.2017.2703620](https://doi.org/10.1109/COMST.2017.2703620).
- [18] A. Jiménez, F. Zampella, and F. Seco, "Improving inertial pedestrian dead-reckoning by detecting unmodified switched-on lamps in buildings," *Sensors*, vol. 14, no. 1, pp. 731–769, Jan. 2014, doi: [10.3390/s140100731](https://doi.org/10.3390/s140100731).
- [19] A. G. Ferreira, D. Fernandes, A. P. Catarino, A. M. Rocha, and J. L. Monteiro, "A loose-coupled fusion of inertial and UWB assisted by a decision-making algorithm for localization of emergency responders," *Electronics*, vol. 8, no. 12, p. 1463, Dec. 2019, doi: [10.3390/electronics8121463](https://doi.org/10.3390/electronics8121463).
- [20] L. Zwirello, X. Li, T. Zwick, C. Ascher, S. Werling, and G. F. Trommer, "Sensor data fusion in UWB-supported inertial navigation systems for indoor navigation," in *Proc. IEEE Int. Conf. Robot. Autom.*, Karlsruhe, Germany, May 2013, pp. 3154–3159, doi: [10.1109/ICRA.2013.6631016](https://doi.org/10.1109/ICRA.2013.6631016).
- [21] Y. Cho, M. Ji, J. Kim, and J. Jeon, "High-scalable 3D indoor positioning algorithm using loosely-coupled Wi-Fi/sensor integration," in *Proc. 17th Int. Conf. Adv. Commun. Tech. (ICACT)*, PyeongChang, South Korea, 2015, pp. 96–99, doi: [10.1109/ICACT.2015.7224765](https://doi.org/10.1109/ICACT.2015.7224765).
- [22] J. Le Scornec, M. Ortiz, and V. Renaudin, "Foot-mounted pedestrian navigation reference with tightly coupled GNSS carrier phases, inertial and magnetic data," in *Proc. Int. Conf. Indoor Position. Indoor Navig. (IPIN)*, 2017, pp. 1–8, doi: [10.1109/IPIN.2017.8115882](https://doi.org/10.1109/IPIN.2017.8115882).
- [23] J. Qian, Y. Cheng, R. Ying, and P. Liu, "A novel indoor localization method based on image retrieval and dead reckoning," *Appl. Sci.*, vol. 10, no. 11, p. 3803, May 2020, doi: [10.3390/app10113803](https://doi.org/10.3390/app10113803).
- [24] J.-O. Nilsson, D. Zachariah, I. Skog, and P. Händel, "Cooperative localization by dual foot-mounted inertial sensors and inter-agent ranging," *EURASIP J. Adv. Signal Process.*, vol. 2013, no. 1, Dec. 2013, Art. no. 164, doi: [10.1186/1687-6180-2013-164](https://doi.org/10.1186/1687-6180-2013-164).
- [25] R. Harle, "A survey of indoor inertial positioning systems for pedestrians," *IEEE Commun. Surveys Tuts.*, vol. 15, no. 3, pp. 1281–1293, 3rd Quart., 2013, doi: [10.1109/SURV.2012.121912.00075](https://doi.org/10.1109/SURV.2012.121912.00075).
- [26] P. Chen, Y. Kuang, and X. Chen, "A UWB/improved PDR integration algorithm applied to dynamic indoor positioning for pedestrians," *Sensors*, vol. 17, no. 9, p. 2065, 2017, doi: [10.3390/s17092065](https://doi.org/10.3390/s17092065).
- [27] H. Yang, Y. Kuang, M. Wang, X. Bao, and Y. Yang, "Indoor mobile localization based on a tightly coupled UWB/INS integration," in *Proc. 16th Int. Conf. Control, Autom., Robot. Vis. (ICARCV)*, Shenzhen, China, Dec. 2020, pp. 1354–1359, doi: [10.1109/ICARCV50220.2020.9305307](https://doi.org/10.1109/ICARCV50220.2020.9305307).
- [28] M. Bloesch, S. Omari, M. Hutter, and R. Siegwart, "Robust visual inertial odometry using a direct EKF-based approach," in *Proc. IEEE/RSJ Int. Conf. Intell. Robots Syst. (IROS)*, Hamburg, Germany, Sep. 2015, pp. 298–304, doi: [10.1109/IROS.2015.7353389](https://doi.org/10.1109/IROS.2015.7353389).
- [29] D. P. Koch, D. O. Wheeler, R. W. Beard, T. W. McLain, and K. M. Brink, "Relative multiplicative extended Kalman filter for observable GPS-denied navigation," *Int. J. Robot. Res.*, vol. 39, no. 9, pp. 1085–1121, Aug. 2020, doi: [10.1177/0278364920903094](https://doi.org/10.1177/0278364920903094).
- [30] N. Decarli, D. Dardari, S. Gezici, and A. A. D'Amico, "LOS/NLOS detection for UWB signals: A comparative study using experimental data," in *Proc. 5th Int. Symp. Wireless Pervasive Comput.*, Modena, Italy, May 2010, pp. 169–173, doi: [10.1109/ISWPC.2010.5483704](https://doi.org/10.1109/ISWPC.2010.5483704).
- [31] S. Yang and M. Baum, "Second-order extended Kalman filter for extended object and group tracking," in *Proc. 19th Int. Conf. Inf. Fusion*, Berlin, Germany, Jul. 2016, pp. 1178–1184.
- [32] G. Rigatos, P. Siano, T. Ghosh, and B. Xin, "A nonlinear optimal control approach for industrial production under an oligopoly model," *IEEE Syst. J.*, vol. 13, no. 2, pp. 1991–2000, Jun. 2019, doi: [10.1109/JSYST.2018.2866431](https://doi.org/10.1109/JSYST.2018.2866431).
- [33] Z. Zheng, S. J. Baek, D. H. Yu, and K. T. Chong, "Comparison study of the Taylor series based discretization method for nonlinear input-delay systems," in *Proc. Austral. Control Conf.*, Fremantle, WA, Australia, 2013, pp. 397–402, doi: [10.1109/AUCC.2013.6697306](https://doi.org/10.1109/AUCC.2013.6697306).
- [34] D. Ghosh, V. Honkote, and K. Narayanan, "Dynamic adaption of noise covariance for accurate indoor localization of mobile robots in non-line-of-sight environments," in *Proc. IEEE Int. Conf. Multisensor Fusion Integr. Intell. Syst. (MFI)*, Karlsruhe, Germany, Sep. 2020, pp. 387–393, doi: [10.1109/MFI49285.2020.9235245](https://doi.org/10.1109/MFI49285.2020.9235245).
- [35] S. Ishibashi, "A compact and high-performance INS for underwater vehicle developed with homegrown technology," in *Proc. IEEE Int. Underwater Tech. Sym. (UT)*, Tokyo, Japan, Dec. 2013, pp. 1–5, doi: [10.1109/UT.2013.6519895](https://doi.org/10.1109/UT.2013.6519895).
- [36] J. Tiemann, L. Koring, P. Gorczak, and C. Wietfeld, "Improving the robustness of control-grade ultra-wideband localization," *IFAC-Papers Line*, vol. 51, no. 10, pp. 103–108, 2018, doi: [10.1016/j.ifacol.2018.06.244](https://doi.org/10.1016/j.ifacol.2018.06.244).
- [37] Q. Fan, B. Sun, Y. Sun, and X. Zhuang, "Performance enhancement of MEMS-based INS/UWB integration for indoor navigation applications," *IEEE Sensors J.*, vol. 17, no. 10, pp. 3116–3130, May 2017, doi: [10.1109/JSEN.2017.2689802](https://doi.org/10.1109/JSEN.2017.2689802).
- [38] J. Kuang, X. Niu, and X. Chen, "Robust pedestrian dead reckoning based on MEMS-IMU for smartphones," *Sensors*, vol. 18, no. 5, p. 1391, 2018, doi: [10.3390/s18051391](https://doi.org/10.3390/s18051391).
- [39] D.-H. Kim and J.-Y. Pyun, "NLOS identification based UWB and PDR hybrid positioning system," *IEEE Access*, vol. 9, pp. 102917–102929, 2021, doi: [10.1109/access.2021.3098416](https://doi.org/10.1109/access.2021.3098416).
- [40] Y.-C. Lai, C.-C. Chang, C.-M. Tsai, S.-C. Huang, and K.-W. Chiang, "A knowledge-based step length estimation method based on fuzzy logic and multi-sensor fusion algorithms for a pedestrian dead reckoning system," *ISPRS Int. J. Geo-Inf.*, vol. 5, no. 5, p. 70, 2016, doi: [10.3390/ijgi5050070](https://doi.org/10.3390/ijgi5050070).
- [41] D. Lim, C. Park, N. H. Kim, S.-H. Kim, and Y. S. Yu, "Fall-detection algorithm using 3-axis acceleration: Combination with simple threshold and hidden Markov model," *J. Appl. Math.*, vol. 2014, Sep. 2014, Art. no. 896030, doi: [10.1155/2014/896030](https://doi.org/10.1155/2014/896030).
- [42] Liu, Li, Wang, and Zhang, "An adaptive UWB/MEMS-IMU complementary Kalman filter for indoor location in NLOS environment," *Remote Sens.*, vol. 11, no. 22, p. 2628, Nov. 2019, doi: [10.3390/rs11222628](https://doi.org/10.3390/rs11222628).
- [43] R. Ali, R. Liu, Y. He, A. Nayyar, and B. Qureshi, "Systematic review of dynamic multi-object identification and localization: Techniques and technologies," *IEEE Access*, vol. 9, pp. 122924–122950, 2021, doi: [10.1109/ACCESS.2021.3108775](https://doi.org/10.1109/ACCESS.2021.3108775).
- [44] R. Liu, Y. He, C. Yuen, B. P. L. Lau, R. Ali, W. Fu, and Z. Cao, "Cost-effective mapping of mobile robot based on the fusion of UWB and short-range 2-D LiDAR," *IEEE/ASME Trans. Mechatronics*, early access, Jun. 9, 2021, doi: [10.1109/TMECH.2021.3087957](https://doi.org/10.1109/TMECH.2021.3087957).
- [45] Y. Zhao, "Performance evaluation of cubature Kalman filter in a GPS/IMU tightly-coupled navigation system," *Signal Process.*, vol. 119, pp. 67–79, Feb. 2016, doi: [10.1016/j.sigpro.2015.07.014](https://doi.org/10.1016/j.sigpro.2015.07.014).
- [46] S. Sczyslo, J. Schroeder, S. Galler, and T. Kaiser, "Hybrid localization using UWB and inertial sensors," in *Proc. IEEE Int. Conf. Ultra-Wideband*, Dec. 2008, pp. 89–92, doi: [10.1109/ICUWB.2008.4653423](https://doi.org/10.1109/ICUWB.2008.4653423).
- [47] S. Pittet, V. Renaudin, B. Merminod, and M. Kasser, "UWB and MEMS based indoor navigation," *J. Navigat.*, vol. 61, no. 3, pp. 369–384, Jul. 2008, doi: [10.1017/s0373463308004797](https://doi.org/10.1017/s0373463308004797).



- [48] X. Li, J. Wang, C. Liu, L. Zhang, and Z. Li, "Integrated WiFi/PDR/Smartphone using an adaptive system noise extended Kalman filter algorithm for indoor localization," *ISPRS Int. J. Geo-Inf.*, vol. 5, no. 2, p. 8, Feb. 2016, doi: [10.3390/ijgi5020008](https://doi.org/10.3390/ijgi5020008).
- [49] R. Liu, F. Liu, C. Liu, and P. Zhang, "Modified sage-husa adaptive Kalman filter-based SINS/DVL integrated navigation system for AUV," *J. Sensors*, vol. 2021, pp. 1–8, Jul. 2021, doi: [10.1155/2021/9992041](https://doi.org/10.1155/2021/9992041).
- [50] Y. Wu, H.-B. Zhu, Q.-X. Du, and S.-M. Tang, "A survey of the research status of pedestrian dead reckoning systems based on inertial sensors," *Int. J. Autom. Comput.*, vol. 16, no. 1, pp. 65–83, 2019, doi: [10.1007/s11633-018-1150-y](https://doi.org/10.1007/s11633-018-1150-y).
- [51] A. R. J. Ruiz, F. S. Granja, J. C. P. Honorato, and J. I. G. Rosas, "Accurate pedestrian indoor navigation by tightly coupling foot-mounted IMU and RFID measurements," *IEEE Trans. Instrum. Meas.*, vol. 61, no. 1, pp. 178–189, Jan. 2012, doi: [10.1109/TIM.2011.2159317](https://doi.org/10.1109/TIM.2011.2159317).
- [52] N. A. Anbu and D. Jayaprassanth, "Integration of inertial navigation system with global positioning system using extended Kalman filter," in *Proc. Int. Conf. Smart Syst. Inventive Technol. (ICSSIT)*, Nov. 2019, pp. 789–794, doi: [10.1109/icssit46314.2019.8987949](https://doi.org/10.1109/icssit46314.2019.8987949).
- [53] J. Youssef, B. Denis, C. Godin, and S. Lesecq, "Loosely-coupled IR-UWB handset and ankle-mounted inertial unit for indoor navigation," in *Proc. IEEE Int. Conf. Ultra-Wideband (ICUWB)*, Aug. 2011, pp. 160–164, doi: [10.1109/ICUWB.2011.6058817](https://doi.org/10.1109/ICUWB.2011.6058817).
- [54] A. Alarifi, A. M. Al-Salman, M. Alsaleh, and A. Alnafessah, "Ultra wideband indoor positioning technologies: Analysis and recent advances," *Sensors*, vol. 16, no. 5, p. 707, 2016, doi: [10.3390/s16050707](https://doi.org/10.3390/s16050707).
- [55] S. Cardarelli, A. Mengarelli, A. Tigrini, A. Strazza, F. Di Nardo, S. Fioretti, and F. Verdini, "Single IMU displacement and orientation estimation of human center of mass: A magnetometer-free approach," *IEEE Trans. Instrum. Meas.*, vol. 69, no. 8, pp. 5629–5639, Aug. 2020, doi: [10.1109/TIM.2019.2962295](https://doi.org/10.1109/TIM.2019.2962295).
- [56] S. Qiu, H. Zhao, N. Jiang, D. Wu, G. Song, H. Zhao, and Z. Wang, "Sensor network oriented human motion capture via wearable intelligent system," *Int. J. Intell. Syst.*, early access, Sep. 2021, doi: [10.1002/int.22689](https://doi.org/10.1002/int.22689).
- [57] I. Ashraf, M. Kang, S. Hur, and Y. Park, "MINLOC: Magnetic field patterns-based indoor localization using convolutional neural networks," *IEEE Access*, vol. 8, pp. 66213–66227, 2020, doi: [10.1109/ACCESS.2020.2985384](https://doi.org/10.1109/ACCESS.2020.2985384).



**RASHID ALI** received the B.S. degree in computer science from the University of Balochistan, Quetta, Pakistan, in 2011, and the M.S. degree in software engineering from Hamdard University, Karachi, Pakistan, in 2019. He is currently pursuing the Ph.D. degree with the School of Information Engineering, Southwest University of Science and Technology, Mianyang, China. Since 2013, he has been a Lecturer with the Department of Computer Science, University of Turbat. He has authored more than five articles. His research interests include AI (robotics), multi-sensor, and vehicle/object indoor positioning and localization.



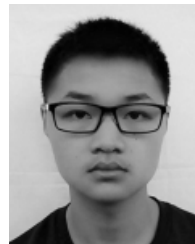
**RAN LIU** received the B.S. degree from the Southwest University of Science and Technology, Mianyang, China, in 2007, and the Ph.D. degree from the University of Tübingen, Tübingen, Germany, in 2014, under the supervision of Prof. Dr. A. Zell and Prof. Dr. A. Schilling. His research interests include robotics, indoor positioning, and SLAM.



**ANAND NAYYAR** received the Ph.D. (computer science) degree from Desh Bhagat University, in 2017, in the area of wireless sensor networks and swarm intelligence. He is currently working with the Graduate School, Duy Tan University, Da Nang, Vietnam. He is also a Certified Professional with more than 75 professional certificates from CISCO, Microsoft, Oracle, Google, Beingcert, EXIN, GAQM, Cyberoam, and many more. He has published more than 450 research papers in various national and international conferences, and international journals (Scopus/SCI/SCIE/SSCI Indexed) with high impact factor. He has authored/coauthored cum edited more than 30 books of computer science. He has five Australian patents to his credit in the area of wireless communications, artificial intelligence, the Internet of Things (IoT), and image processing. He is working in the area of wireless sensor networks, the IoT, swarm intelligence, cloud computing, artificial intelligence, blockchain, cyber security, network simulation, and wireless communications. He was a member of more than 50 associations as a Senior Member and a Life Member, and also acting as an ACM Distinguished Speaker. He was associated with more than 500 international conferences as the programme committee/the chair/the advisory board/a review board member. He was awarded more than 30 awards for teaching and research—the young scientist, the best scientist, the young researcher award, the outstanding researcher award, the excellence in teaching, and many more. He is acting as an Associate Editor for *Wireless Networks* (Springer), *IET Quantum Communication*, *IET Wireless Sensor Systems*, *IET Networks*, *IJDST*, *IJISP*, and *IJCINI*. He is acting as the Editor-in-Chief of IGI-Global and USA Journal *International Journal of Smart Vehicles and Smart Transportation* (IJSVST).



**BASIT QURESHI** (Member, IEEE) received the bachelor's degree in computer science from Ohio University, Athens, OH, USA, in 2000, the master's degree in computer science from Florida Atlantic University, in 2002, and the Ph.D. degree in computer science from the University of Bradford, U.K., in 2011. He is currently an Associate Professor and the Chair of the Department of Computer Science, Prince Sultan University, Saudi Arabia. He has published over 60 research works in the area of robotics, the Internet of Things, machine learning, and computational intelligence. He is a member of the IEEE Computer Society, the IEEE Communications Society, and ACM.



**ZHIQIANG CAO** received the B.S. degree from the Southwest University of Science and Technology, Mianyang, China, in 2019, where he is currently pursuing the M.A.Sc. degree with the School of Information Engineering. His research interests include indoor localization, SLAM, and UWB.

...